Supporting Information

The role of LMCT state on luminescence quenching in dimeric lanthanide dipivaloylmethanate compounds

Paulo R. S. Santos.[a] Ashely A. S. S. Jesus.[a] William B. Lima.[a]. Iran F. Silva.[a] Joaldo G. Arruda.[a] Wagner M. Faustino.[a] Maria Claudia F. C. Felinto.[b] Hermi F. Brito.[c] Israel F. Costa.[c] Renata Diniz[d]. Ercules E.S. Teotonio.[a,]*

[a]Departamento de Química-Universidade Federal da Paraíba. 58051-970. João Pessoa -PB.Brazil.

[b]Nuclear and Energy Research Institute–IPEN/CNEN. 05508-900. São Paulo–SP. Brazil

[c]Departamento de Química Fundamental - Instituto de Química da Universidade de São Paulo. 05508-900. São Paulo - SP.Brazil.

[d]Department of Chemistry. ICEx. University of Minas Gerais. Belo Horizonte. MG. 31270-901. Brazil

Contents

1. Figures

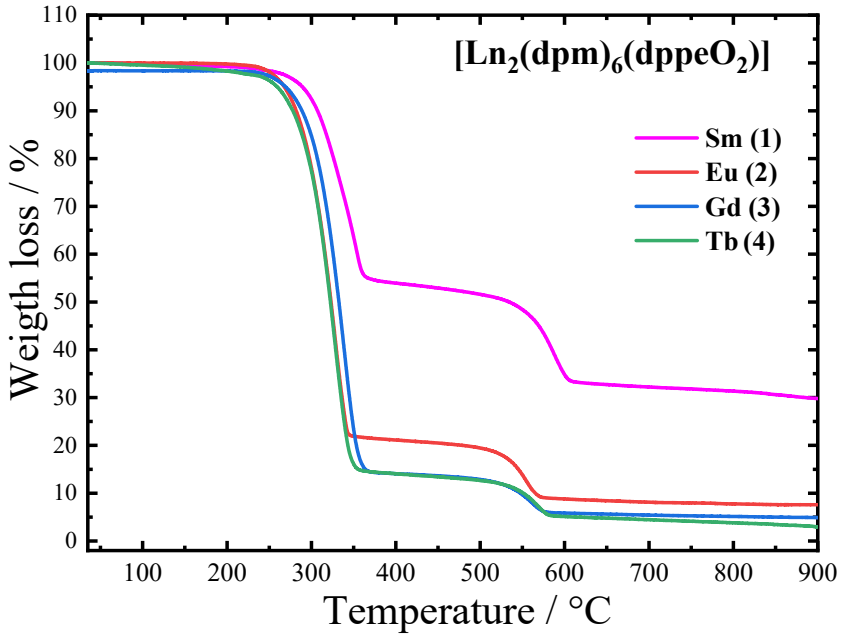

Figure S1. Thermogravimetric analysis curves of the $[Ln_2(dpm)_6(dppeO_2)]$ complexes. where Ln: Sm(1). Eu(2). Gd(3) and Tb(4). recorded in the 30 - 900 °C interval. under dynamic N_2 atmosphere.

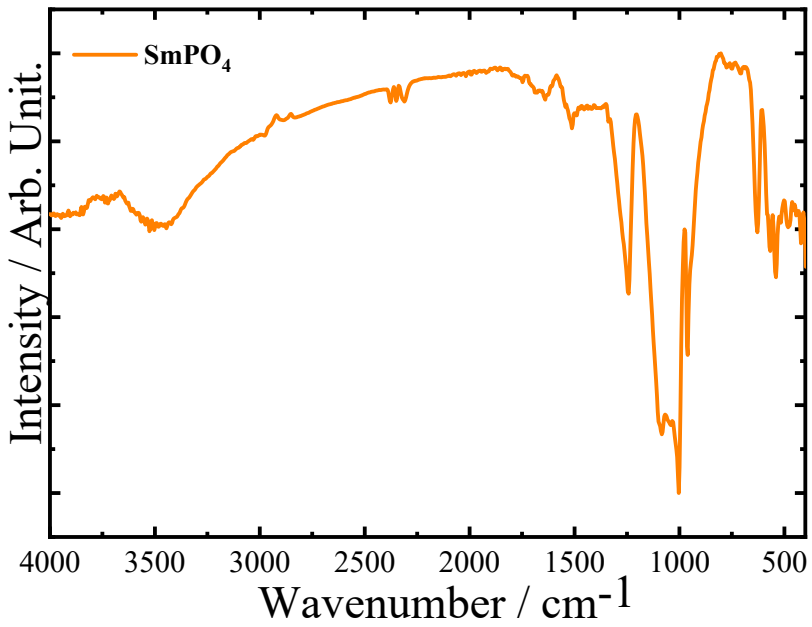

Figure S2. Absorption spectra in the infrared region of the $SmPO_4$ recorded in the range of 400 – 4000 cm^{-1} in KBr.

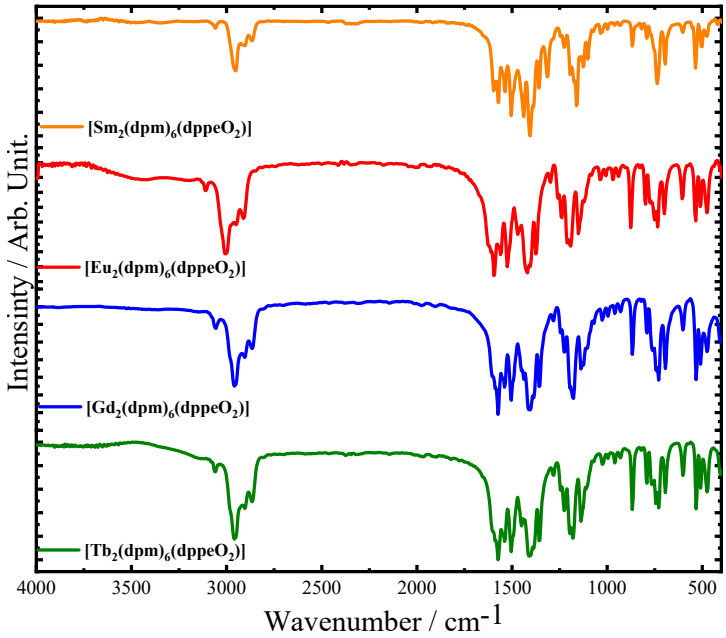

Figure S3. Absorption spectra in the infrared region of the complexes $[Ln_2(dpm)_6(dppeO_2)]$ (where Ln: Sm^{3+}. Eu^{3+}. Gd^{3+} and Tb^{3+}) recorded in the range of 400 – 4000 cm^{-1} in KBr.

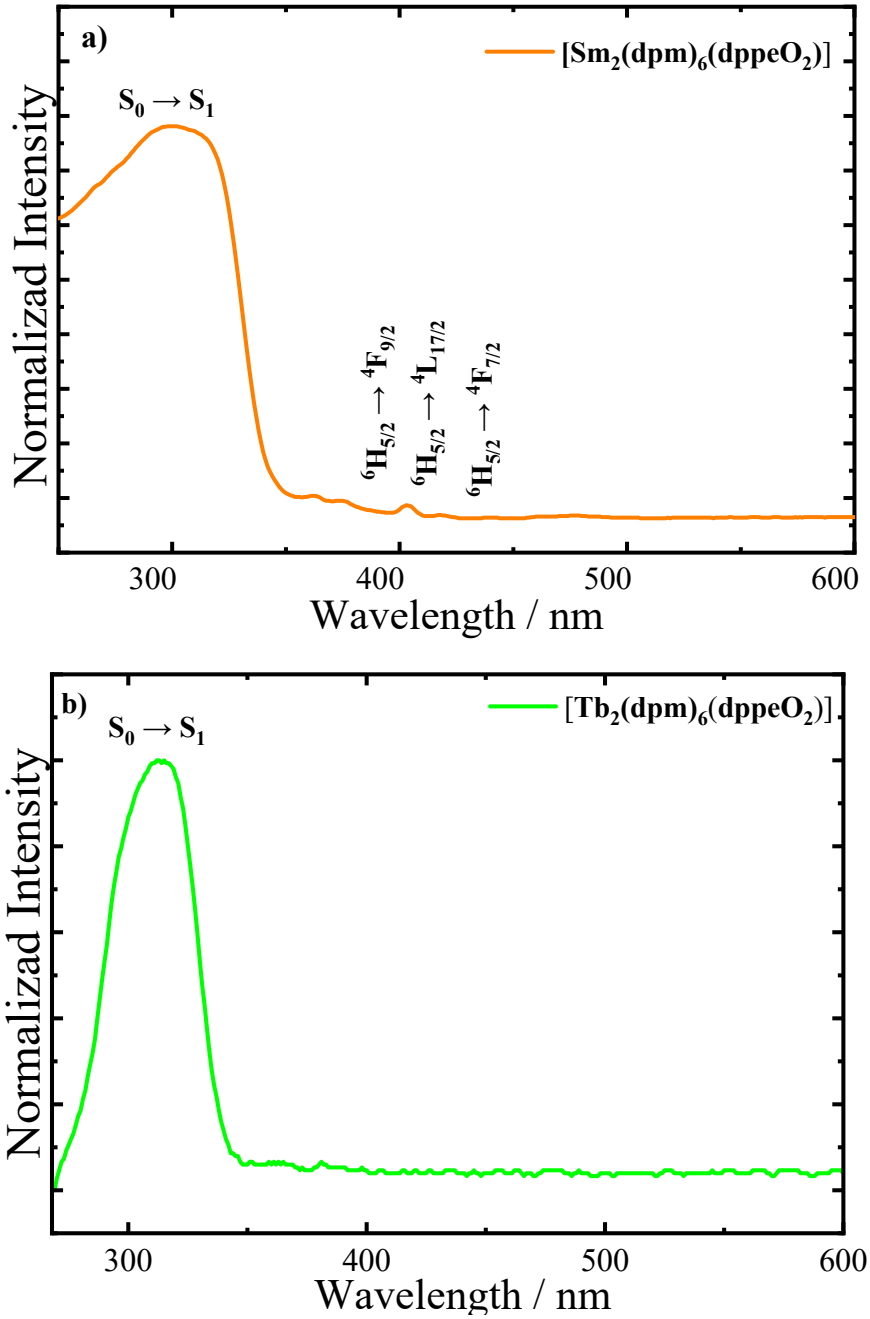

Figure S4. Reflectance spectra of the complexes a) $[Sm_2(dpm)_6(dppeO_2)]$ and b) $[Tb_2(dpm)_6(dppeO_2)]$ in the solid state. recorded in the range of 200 to 600 nm.

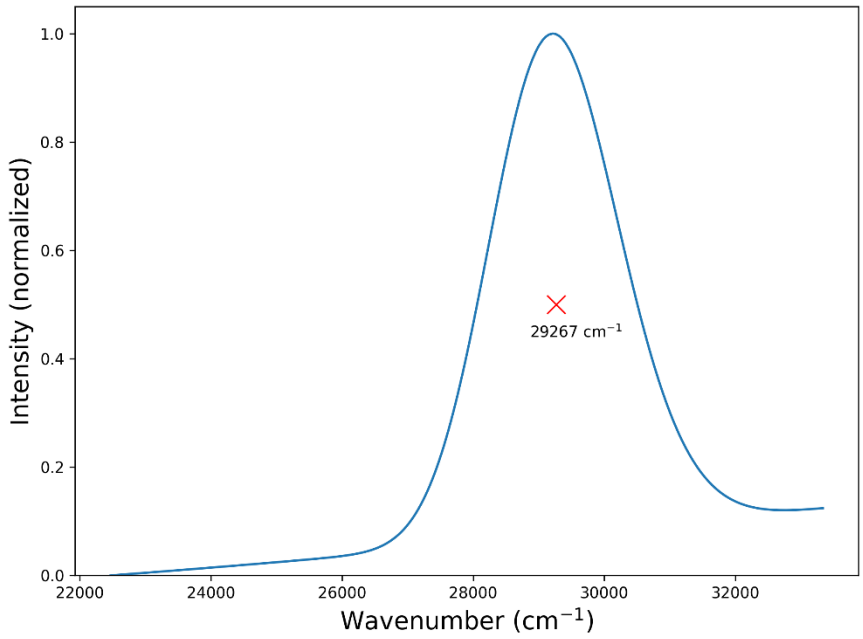

Figure S5. Jacobian transform spectral data of the deconvoluted LMCT band of the $[Eu_2(dpm)_6(dppeO_2)]$ compound.

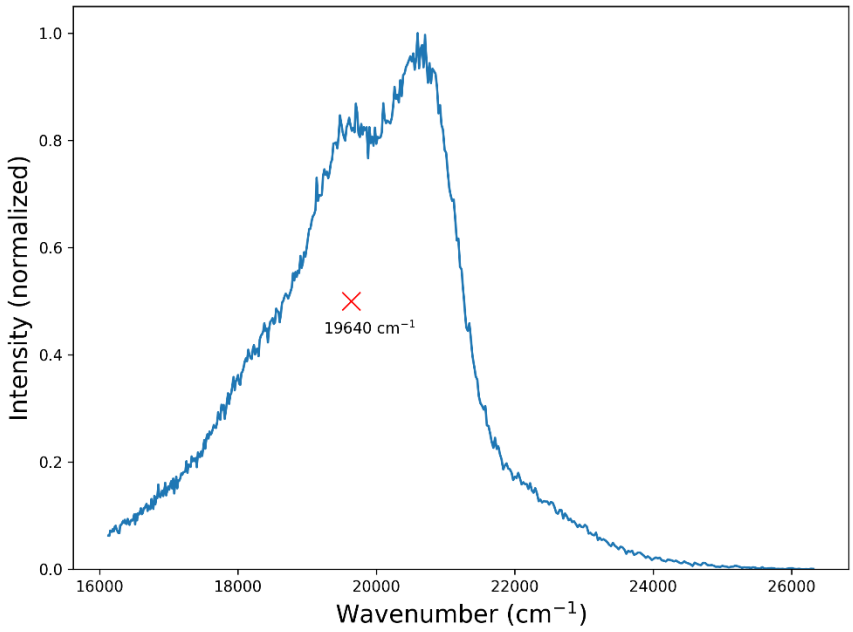

Figure S6. Jacobian transform spectral data of the phosphoresecence band of the $[Gd_2(dpm)_6(dppeO_2)]$ compound.

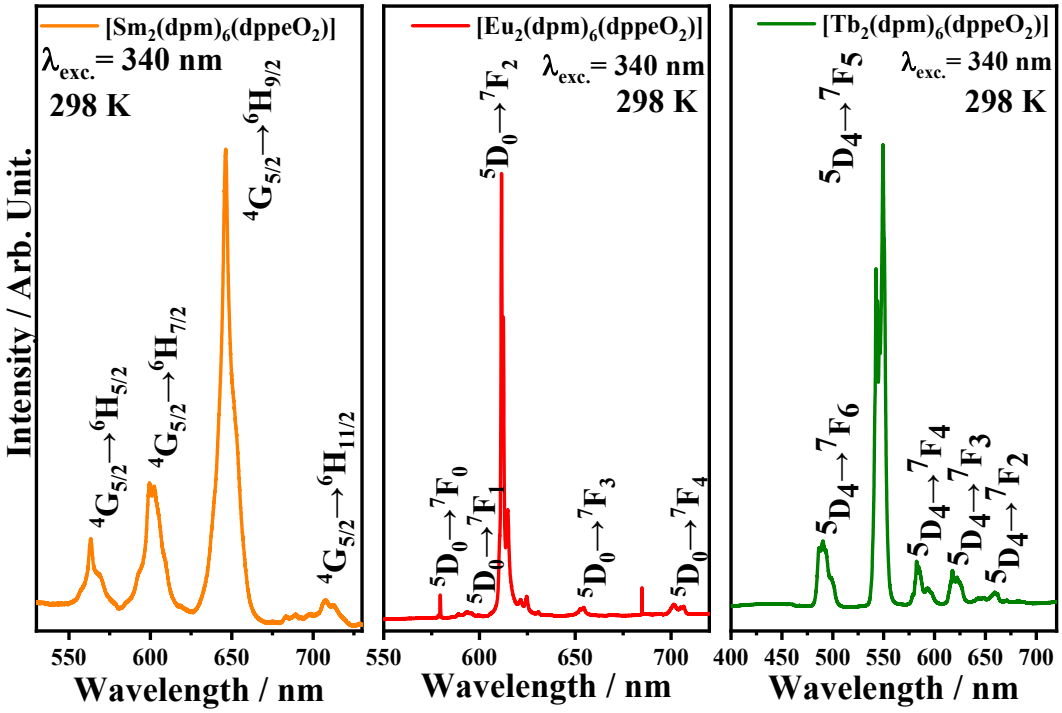

Figure S7. Emission spectra of the complexes $[Ln_2(dpm)_6(dppeO_2)]$ (where Ln: Sm^{3+}. Eu^{3+} and Tb^{3+}) recorded at a) 298 K.

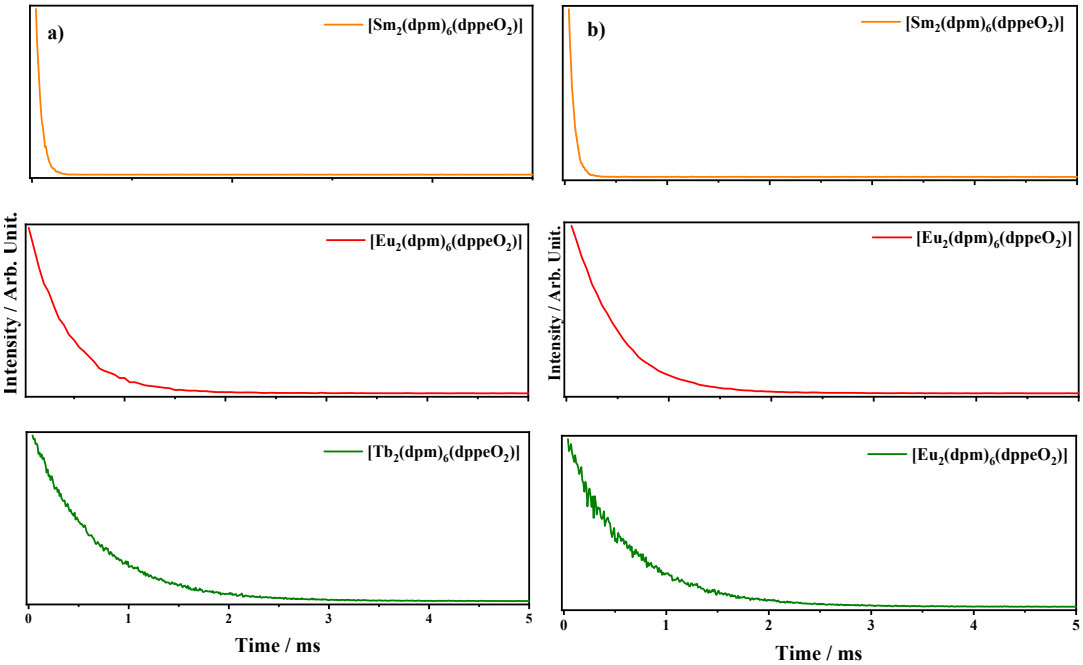

Figure S8. Luminescence decay curves of the complexes $[Ln_2(dpm)_6(dppeO_2)]$ (where Ln: Sm^{3+}. Eu^{3+} and Tb^{3+}) recorded at a) 298 K and b) 77 K monitoring the emission of Ln^{3+} with excitation at 350 nm.

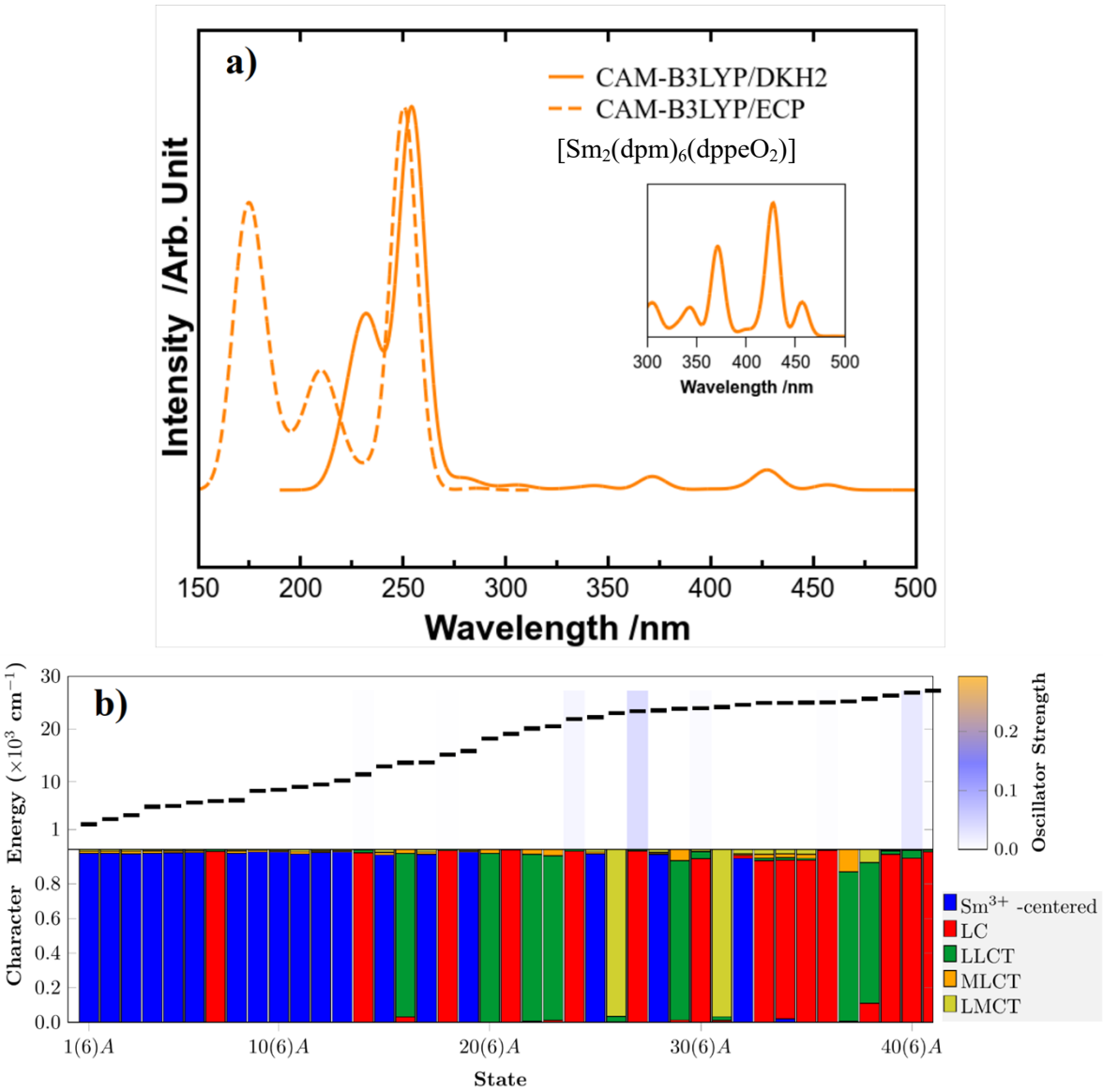

Figure S9: a) Absorption spectrum in the ultraviolet region obtained via DT-DFT/CAM-B3LYP/def2-SVP level using the relativistic Hamiltonian DKH2 for the coordination compound [$Sm_2(dpm)_6(dppeO_2)$] and b) Analysis of excited states using TheoDORE.

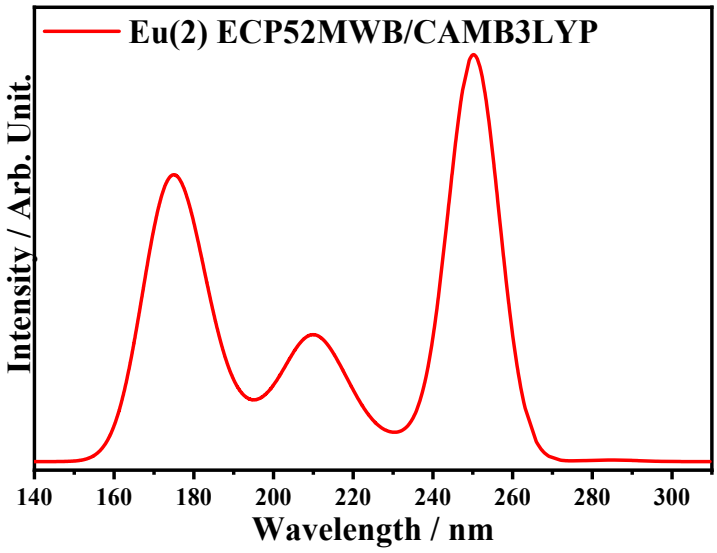

Figure S10. Absorption spectra in the ultraviolet region obtained via TD-DFT ECP

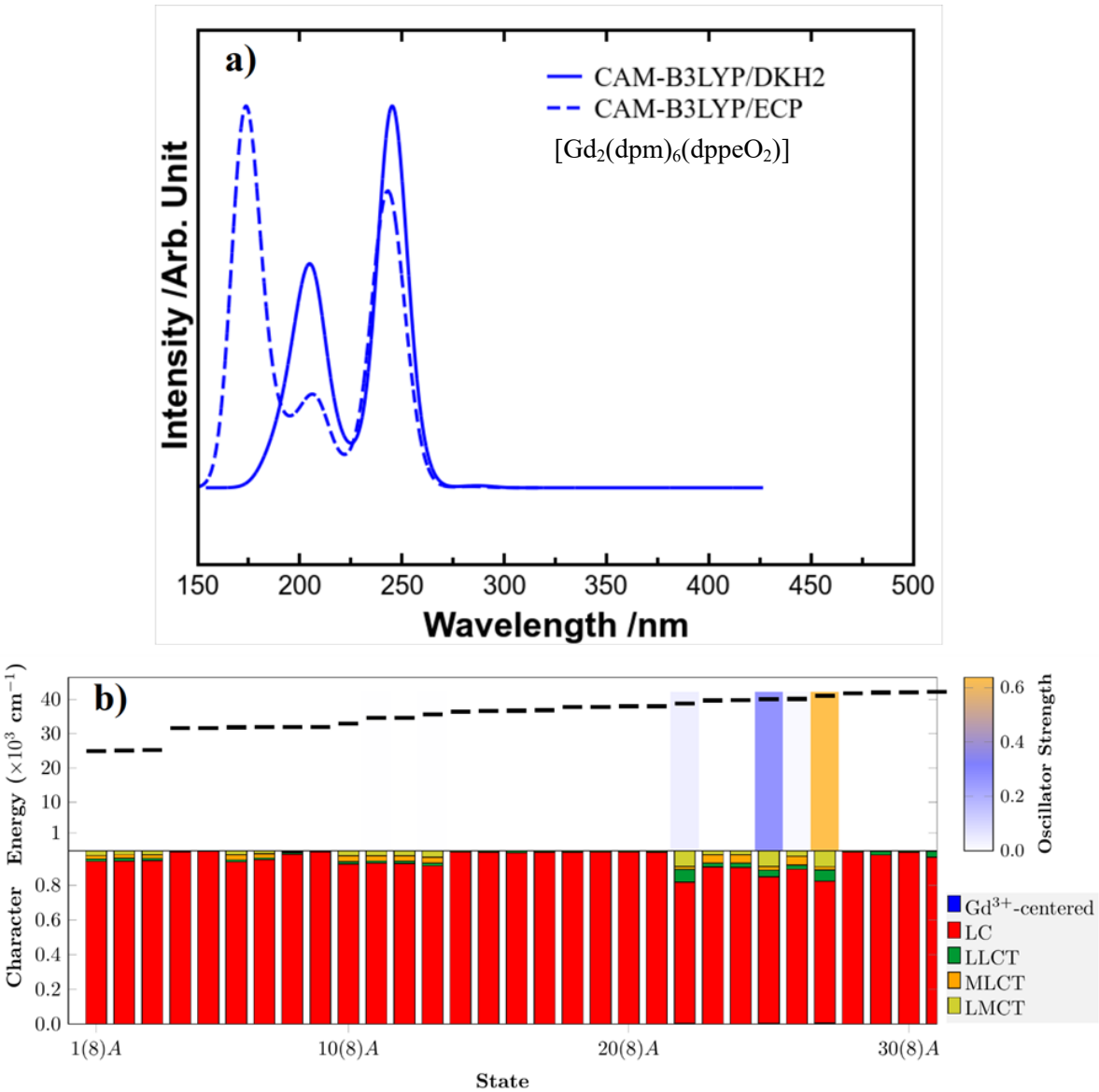

Figure S11: a) Absorption spectrum in the ultraviolet region obtained via DT-DFT/CAM-B3LYP/def2-SVP level using the relativistic Hamiltonian DKH2 for the coordination compound [$Gd_2(dpm)_6(dppeO_2)$] and b) Analysis of excited states using TheoDORE.

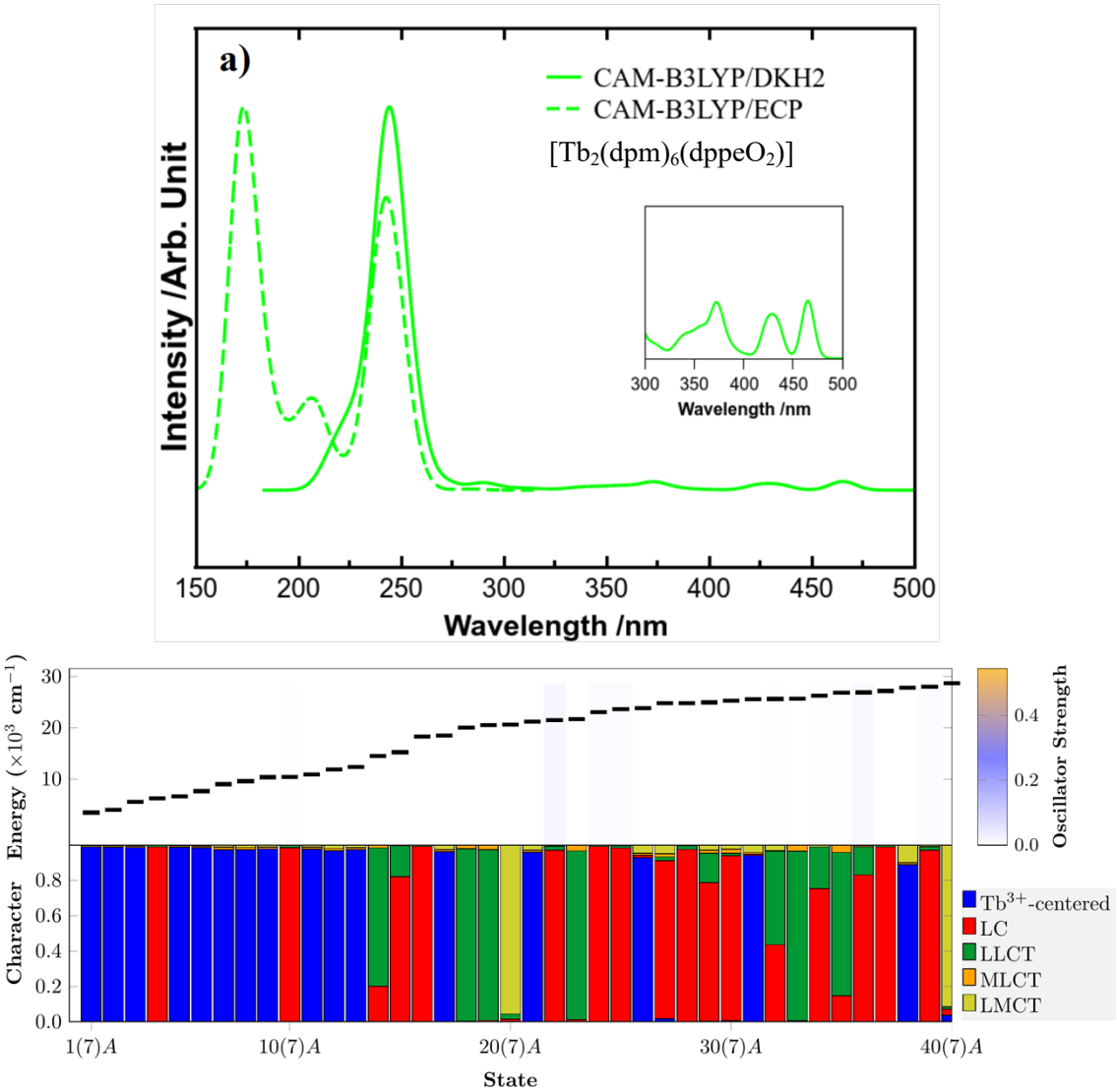

Figure S12: a) Absorption spectrum in the ultraviolet region obtained via DT-DFT/CAM-B3LYP/def2-SVP level using the relativistic Hamiltonian DKH2 for the coordination compound [$Tb_2(dpm)_6(dppeO_2)$] and b) Analysis of excited states using TheoDORE.

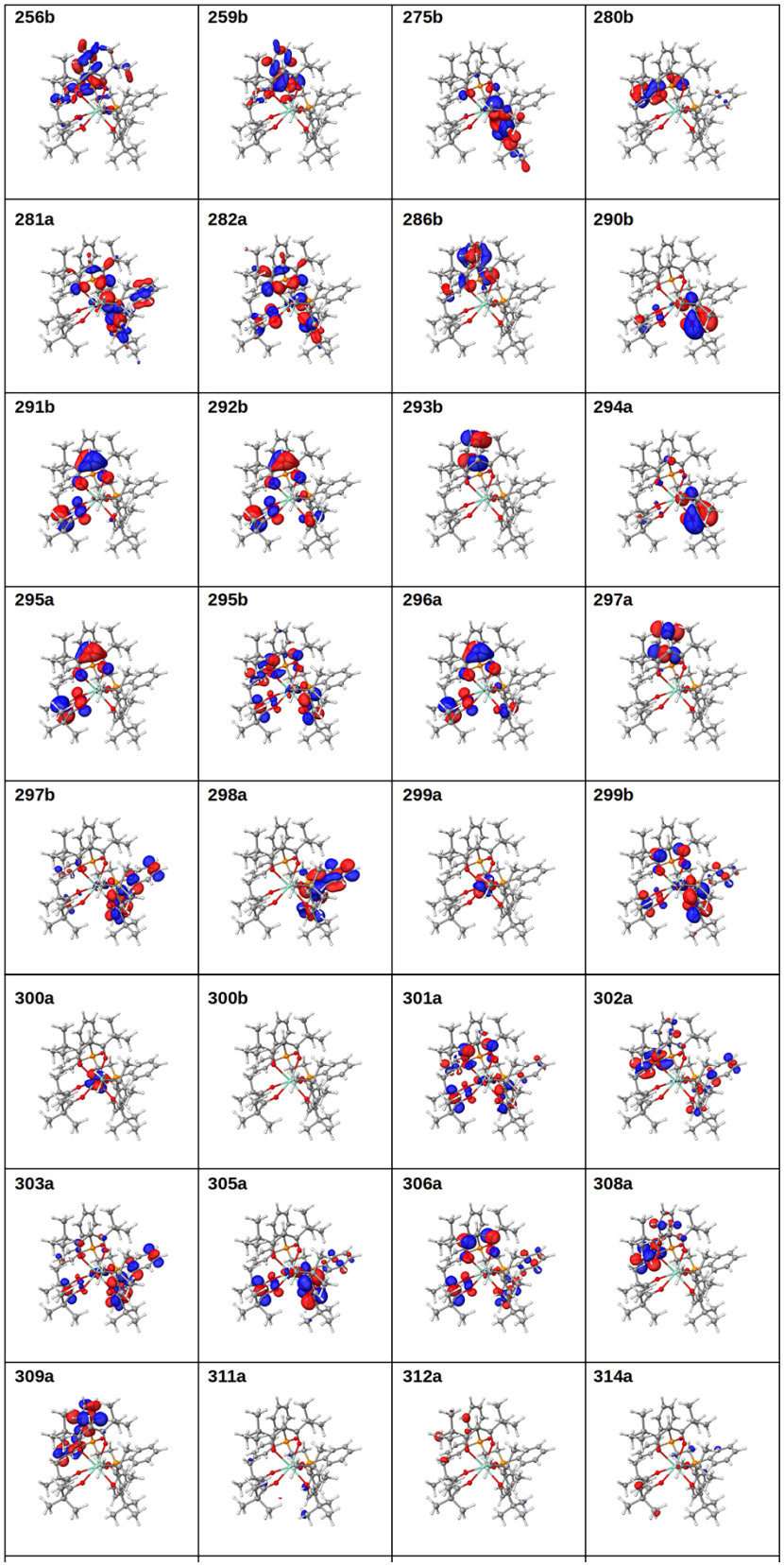

Figure S13. CAM-B3LYP/DKH2 Khon-Sham orbitals for the coordination compound $[Sm_2(dpm)_6(dppeO_2)]$ (a for alpha and b for beta) for the above monoelectronic transitions, isovalue=0.04.

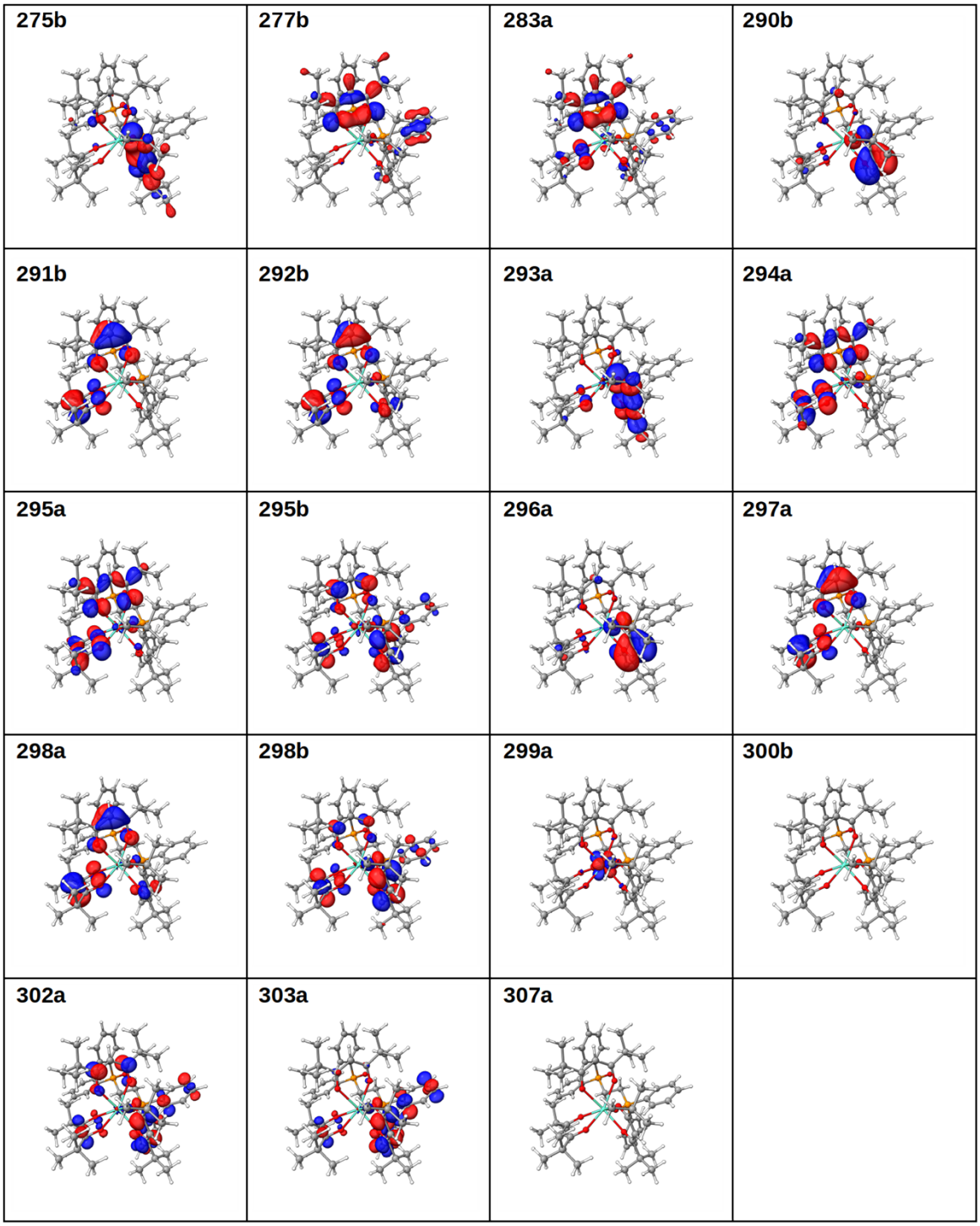

Figure S14 CAM-B3LYP/DKH2 Khon-Sham orbitals for the coordination compound $[Eu_2(dpm)_6(dppeO_2)]$ (a for alpha and b for beta) for the above monoelectronic transitions, isovalue=0.04.

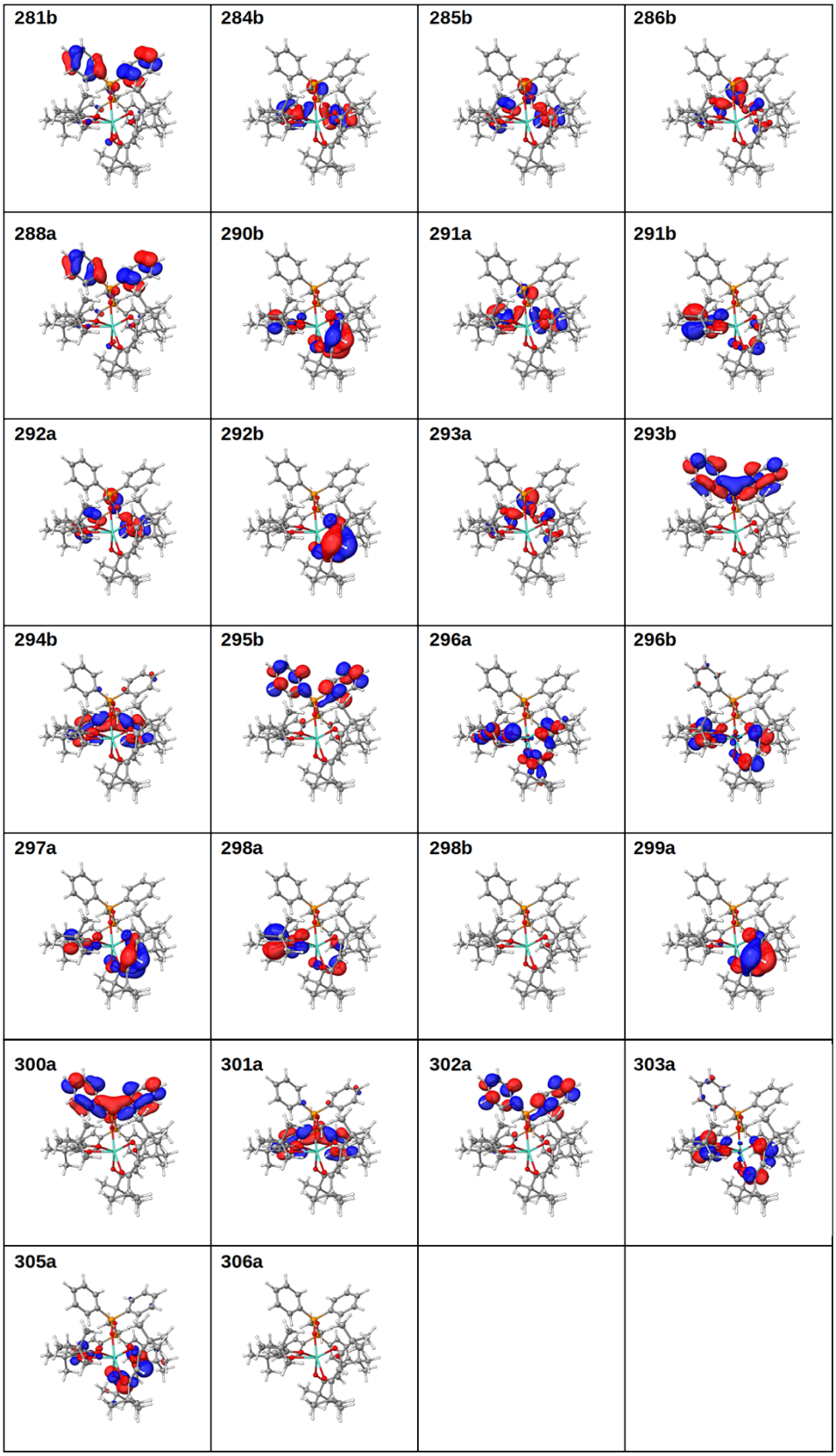

Figure S15. CAM-B3LYP/DKH2 Khon-Sham orbitals for the coordination compound $[Gd_2(dpm)_6(dppeO_2)]$ (a for alpha and b for beta) for the above monoelectronic transitions, isovalue=0.04.

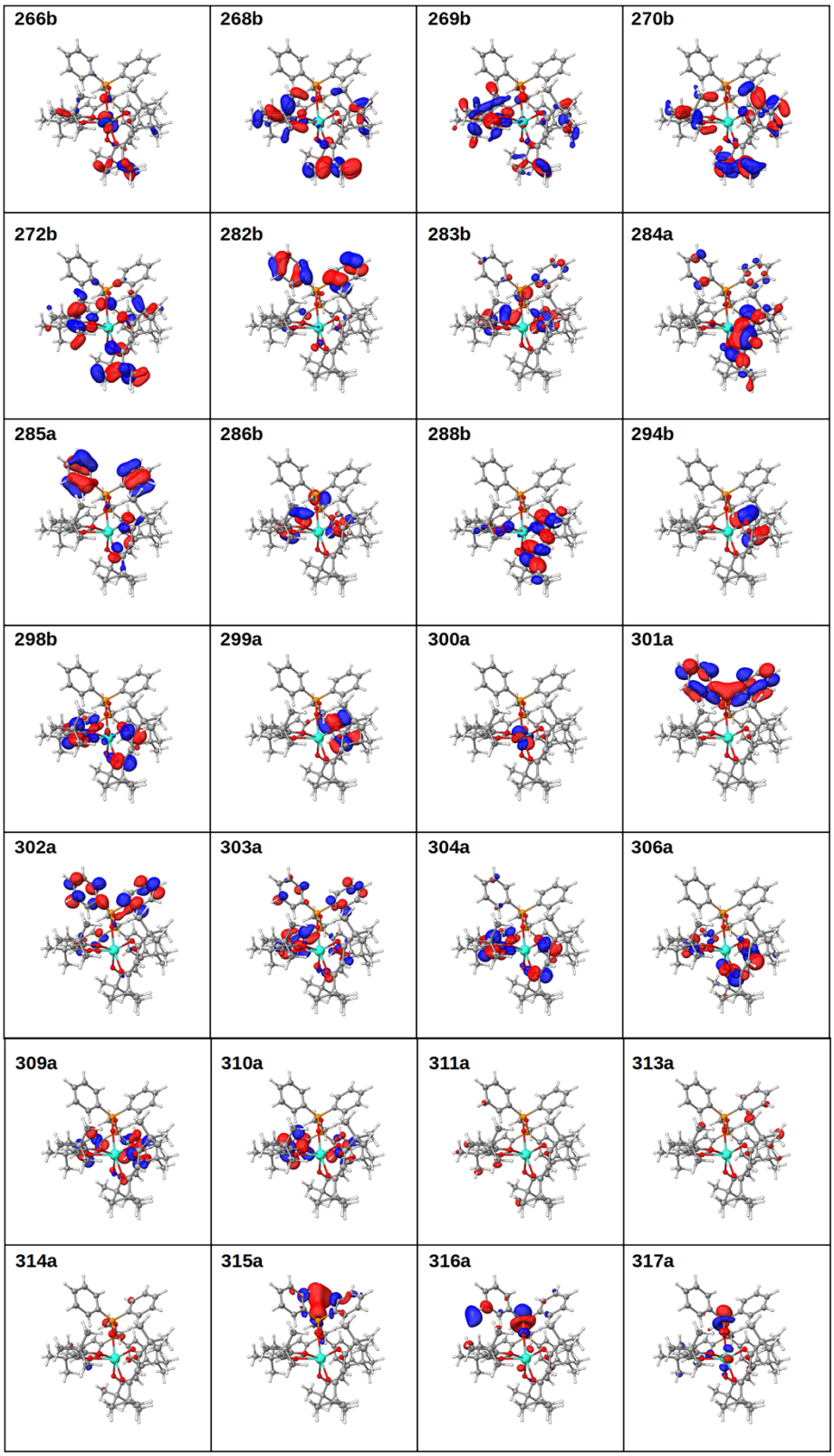

Figure S16. CAM-B3LYP/DKH2 Khon-Sham orbitals for the coordination compound $[Tb_2(dpm)_6(dppeO_2)]$ (a for alpha and b for beta) for the above monoelectronic transitions, isovalue=0.04.

2. Tables

Table S1. Main geometric parameters of Eu, Gd and Tb crystals.

Bond distance / Å			
	Eu	Gd	Tb
Ln-O1	2.312(3)	2.332(4)	2.264(2)
Ln-O2	2.402(2)	2.346(4)	2.310(3)
Ln-O3	2.351(2)	2.321(4)	2.323(3)
Ln-O4	2.340(4)	2.304(5)	2.345(3)
Ln-O5	2.294(3)	2.279(4)	2.300(2)
Ln-O6	2.350(2)	2.330(4)	2.325(3)
Ln-O7	2.342(3)	2.305(4)	2.290(3)
Bond angle / °			
	Eu	Gd	Tb
O1-Ln-O2	125.43(9)	130.57(16)	81.24(10)
O1-Ln-O3	77.31(9)	80.67(15)	130.15(11)
O1-Ln-O4	91.86(9)	78.31(16)	84.87(11)
O1-Ln-O5	153.1(1)	130.32(17)	151.02(10)
O1-Ln-O6	91.5(1)	134.31(17)	74.59(10)
O1-Ln-O7	72.6(1)	70.94(17)	81.99(12)
O2-Ln-O3	75.56(8)	71.27(16)	79.91(10)
O2-Ln-O4	71.27(8)	77.55(16)	72.11(10)
O2-Ln-O5	81.29(9)	81.95(19)	145.37(11)
O2-Ln-O6	124.74(9)	114.40(16)	130.75(11)
O2-Ln-O7	144.69(9)	145.02(17)	134.72(11)
O3-Ln-O4	129.27(8)	85.16(18)	114.20(10)
O3-Ln-O5	117.06(9)	81.37(16)	78.18(10)
O3-Ln-O6	74.88(9)	150.58(17)	177.61(10)
O3-Ln-O7	139.50(9)	74.17(16)	80.02(10)
O4-Ln-O5	94.67(9)	79.92(16)	81.26(12)
O4-Ln-O6	155.69(9)	157.8(2)	124.22(13)
O4-Ln-O7	78.70(9)	123.9(2)	71.75(11)
O5-Ln-O6	72.4(1)	105.9(2)	156.73(13)
O5-Ln-O7	83.1(1)	81.92(19)	105.72(13)
O6-Ln-O7	79.4(1)	77.2(2)	76.78(13)

Table S2. Shape analysis of $[Ln_2(dpm)_6(dppeO_2)]$ using SHAPE 2.1. The values in the table are the continuous measurements (CShM. dimensionless) for each idealized geometry.

Ideal Geometry	Code	point group	Gd^{3+}	Eu^{3+}	Tb^{3+}
Heptagonal	HP-7	D_{7d}	34.34	33.58	34.31
Hexagonal Pyramid	HPY-7	C_{6v}	19.95	20.36	20.07
Pentagonal Pyramid	PBPY-7	D_{5h}	6.850	6.077	6.686
Capped Octahedron	COC-7	C_{3v}	0.537	2.165	0.499
Trigonal Capped Prism	CTPT-7	C_{2v}	1.127	0.724	1.069

Table S3. Temperature ranges and melting points of the coordination compounds of bis(phosphinoxides) compounds in an N_2 atmosphere.

Compound	ΔT-1 (°C)	Δm (%)	ΔT-2 (°C)	Δm (%)	T_f (DSC) (°C)	Residue Cal. (%)	Residue Found (%)
$[Sm_2(dpm)_6(dppeO_2)]$	237-390	45	508-630	19	242	30	32
$[Eu_2(dpm)_6(dppeO_2)]$	222-367	78	497-593	11	237	19	13
$[Gd_2(dpm)_6(dppeO_2)]$	231-386	85	456-601	8	237	20	5
$[Tb_2(dpm)_6(dppeO_2)]$	224-378	83	504-609	8	274	20	3

Table S4. Parameters for the first coordination sphere of the Eu^{3+} ion in the $[Eu_2(dpm)_6(dppeO_2)]$ dimeric complex. where $d(Eu^{3+}\text{-}O)$ corresponds to the Eu^{3+}-O bonding lengths (in Å). g is the charge factor and. α' (in $Å^3$) and α_{OP} (in 10^{-2} $Å^3$) are the effective and overlap polarizabilities. Respectively.

Atom	$d(Eu^{3+}\text{-}O)$ (Å)	g ($Å^3$)	α' ($Å^3$)	α_{OP} (10^{-2} $Å^3$)
O(1)-dpm	2.312043	0.724	0.634	4.349
O(2)-dpm	2.401675	0.555	0.404	3.705
O(3)-dpm	2.340417	0.724	0.634	4.137
O(4)-dpm	2.350379	0.555	0.404	4.065
O(5)-dpm	2.294030	0.724	0.634	4.487
O(6)-dpm	2.341735	0.555	0.404	4.128
O(7)-$dppeO_2$	2.351447	0.929	1.539	4.057

Table S5. Parameters for the first coordination sphere of the Eu^{3+} ion in the $[Tb_2(dpm)_6(dppeO_2)]$ dimeric complex. where d(Tb^{3+}-O) corresponds to the Eu^{3+}-O bonding lengths (in Å). g is the charge factor and. α' (in $Å^3$) and α_{OP} (in 10^{-2} $Å^3$) are the effective and overlap polarizabilities, respectively.

Atom	d(Tb^{3+}-O)	g	α'	α_{OP}
	(Å)	($Å^3$)	($Å^3$)	(10^{-2} $Å^3$)
O(1)-dpm	2.264232	0.581	0.815	5.375
O(2)-dpm	2.310346	0.599	0.412	4.970
O(3)-dpm	2.323405	0.581	0.815	4.860
O(4)-dpm	2.345238	0.599	0.412	4.695
O(5)-dpm	2.300024	0.581	0.815	5.061
O(6)-dpm	2.324718	0.599	0.412	4.853
O(7)-$dppeO_2$	2.290246	1.017	1.731	5.145

Table S6. Parameters for the first coordination sphere of the Eu^{3+} ion in the $[Sm_2(dpm)_6(dppeO_2)]$ dimeric complex. where d(Sm^{3+}-O) corresponds to the Eu^{3+}-O bonding lengths (in Å). g is the charge factor and. α' (in $Å^3$) and α_{OP} (in x10^{-2} $Å^3$) are the effective and overlap polarizabilities, respectively.

Atom	d(Sm^{3+}-O)	g	α'	α_{OP}
	(Å)	($Å^3$)	($Å^3$)	(10^{-2} $Å^3$)
O(1)-dpm	2.303884	0.103	0.083	4.455
O(2)-dpm	2.331192	0.125	0.187	4.267
O(3)-dpm	2.345445	0.103	0.083	4.171
O(4)-dpm	2.320672	0.125	0.187	4.339
O(5)-dpm	2.279259	0.103	0.083	4.630
O(6)-dpm	2.330140	0.125	0.187	4.274
O(7)-$dppeO_2$	2.304205	0.982	1.755	4.453

Supporting Information

Table S7. Experimental and theoretical intensity parameters (Ω_λ, λ = 2,4 and 6) and their contributions FED and DC (in 10^{-20} cm^2) and the general relative error f_{error} (dimensionless).

[$Tb_2(dpm)_6(dppeO_2)$]					
Ω_λ (10^{-20} cm^2)	**Experimental** (10^{-20} cm^2)	**Theoretical** (10^{-20} cm^2)	**FED** (10^{-20} cm^2)	**DC** (10^{-20} cm^2)	f_{error} (dimensionless)
Ω_2	26.8	26.8	0.133	24.1	0
Ω_4	7.3	7.2	0.152	5.53	0.01
Ω_6	1	0.9	0.219	0.4	0.1
[$Sm_2(dpm)_6(dppeO_2)$]					
Ω_λ (10^{-20} cm^2)	**Experimental** (10^{-20} cm^2)	**Theoretical** (10^{-20} cm^2)	**FED** (10^{-20} cm^2)	**DC** (10^{-20} cm^2)	f_{error} (dimensionless)
Ω_2	26.8	26.7	0.43	23.2	0.003
Ω_4	7.3	7.3	0.12	6.1	0
Ω_6	1	1.3	0.24	0.7	0.3

Table S8. Direct IET rates (W^S *and* W^T) and backtransfer (W_B^S *and* W_B^T) in units of (s^{-1}) for complexes [$Tb_2(dpm)_6(dppeO_2)$].

[$Tb_2(dpm)_6(dppeO_2)$]	
Energy Transfer from S_1 state	$W(S^{-1})$
$S_1 \rightarrow (^7F_5 \rightarrow ^5H_4)$	$1{,}60 \cdot 10^{10}$
$S_1 \rightarrow (^7F_6 \rightarrow ^5F_4)$	$9{,}76 \cdot 10^{9}$
Back energy Transfer from S_1 state	
$S_1 \leftarrow (^7F_6 \rightarrow ^5F_5)$	$8{,}75 \cdot 10^{9}$
$S_1 \leftarrow (^7F_5 \rightarrow ^5F_4)$	$1{,}38 \cdot 10^{10}$
Energy Transfer from T_1 state	
$T_1 \rightarrow (^7F_0 \rightarrow ^5D_4)$	$9{,}20 \cdot 10^{8}$
Back energy Transfer from T_1 state	
$T_1 \leftarrow (^7F_5 \rightarrow ^5G_5)$	$9{,}44 \cdot 10^{8}$
$T_1 \leftarrow (^7F_6 \rightarrow ^5G_6)$	$1{,}23 \cdot 10^{9}$

Table S9. Direct IET rates (W^S *and* W^T) and backtransfer (W_B^S *and* W_B^T) in units of (s^{-1}) for complexes $[Sm_2(dpm)_6(dppeO_2)]$.

$[Sm_2(dpm)_6(dppeO_2)]$	
Energy Transfer from S_1 state	$W(S^{-1})$
$S_1 \rightarrow (^6H_{3/2} \rightarrow {}^6P_{3/2})$	$5.43 \cdot 10^6$
$S_1 \rightarrow (^6H_{3/2} \rightarrow {}^4F_{3/2})$	$9,.78 \cdot 10^6$
Back energy Transfer from S_1 state	
$S_1 \leftarrow (^6H_{3/2} \rightarrow {}^6P_{7/2})$	$2.32 \cdot 10^{-9}$
Energy Transfer from T_1 state	
$T_1 \rightarrow (^6H_{5/2} \rightarrow {}^4G_{5/2})$	$1.29 \cdot 10^9$
Back energy Transfer from T_1 state	
$T_1 \leftarrow (^6H_{5/2} \rightarrow {}^4F_{5/2})$	$2.52 \cdot 10^8$
$T_1 \leftarrow (^6H_{5/2} \rightarrow {}^4G_{7/2})$	$7.82 \cdot 10^8$

Table S10 Selected CAMB3LYP/DKH2 excited states, oscillator strength and monoelectronic transitions for [$Sm_2(dpm)_6(dppeO_2)$] fragment.

State	Energy /cm^{-1}	λ /nm	fosc	Transitions
24	21882.8	457.0	0.0109	297a→301a (18.3%) 297a→302a (41.4%) 297a→303a (6.9%) 297a→309a (9.0%) 280b→293b (7.7%)
27	23367.7	427.9	0.0405	280b→293b (55.6%) 286b→293b (9.6%)
30	23936.1	417.8	0.0055	297a→298a (89.6%)
40	26914.1	371.6	0.0269	297a→308a (14.3%) 256b→293b (7.7%) 259b→293b (10.9%)
64	32690.1	305.9	0.0055	294a→299a (94.4%)
93	39088.5	255.8	0.2165	295a→301a (12.7%) 295a→303a (5.6%) 295a→305a (5.5%) 291b→295b (8.0%) 292b→300b (9.8%)
94	39217.7	255.0	0.2936	296a→301a (14.3%) 291b→300b (5.6%) 292b→295b (9.0%)
97	39633.4	252.3	0.2138	294a→301a (7.6%) 294a→303a (6.8%) 294a→305a (8.5%) 290b→295b (10.9%) 290b→299b (5.6%)
98	39651.8	252.2	0.0802	281a→305a (5.2%) 275b→295b (7.5%) 275b→297b (5.0%) 275b→299b (12.3%)

Table S11 Selected CAMB3LYP/DKH2 excited states, oscillator strength and monoelectronic transitions for $[Eu_2(dpm)_6(dppeO_2)]$ fragment.

State	Energy /cm^{-1}	λ /nm	fosc	Transitions
8	22264.1	449.2	0.0037	297a→ 299a (94.3%)
9	22762.7	439.3	0.0032	296a→ 299a (94.4%)
13	25884.7	386.3	0.0051	294a→ 299a (33.6%) 295a→ 299a (55.3%)
14	25928.2	385.7	0.0083	294a→ 299a (57.7%) 295a→ 299a (32.5%)
15	26392.7	378.9	0.0074	293a→ 299a (87.7%)
37	39810.6	251.2	0.1996	297a→ 302a (7.1%) 291b→ 295b (5.3%)
38	39828.2	251.1	0.0941	275b→ 295b (6.5%) 275b→ 298b (10.7%) 291b→ 295b (7.8%)
39	39900.2	250.6	0.0465	283a→ 302a (5.1%) 283a→ 307a (5.7%) 277b→ 295b (6.2%) 277b→ 300b (7.3%)
40	39932.2	250.4	0.3593	297a→ 307a (8.5%) 298a→ 302a (12.2%) 291b→ 300b (6.7%) 292b→ 295b (16.8%) 292b→ 298b (5.8%)
41	39976.5	250.1	0.2791	296a→ 302a (8.6%) 296a→ 303a (5.7%) 297a→ 302a (7.2%) 290b→ 295b (11.0%) 290b→ 298b (5.1%) 291b→ 295b (7.1%) 292b→ 300b (5.2%)

Table S12 Selected CAMB3LYP/DKH2 excited states, oscillator strength and monoelectronic transitions for [$Gd_2(dpm)_6(dppeO_2)$] fragment.

State	Energy /cm^{-1}	λ /nm	fosc	Transitions
25	40056.4	249.6	0.2689	297a→303a (10.1%) 298a→303a (9.4%) 298a→306a (6.7%) 290b→296b (9.3%) 291b→296b (10.2%)
27	41024.9	243.8	0.6371	298a→303a (13.8%) 299a→305a (11.4%) 291b→296b (13.5%) 292b→298b (8.9%)
60	47192.2	211.9	0.0344	292a→301a (6.0%) 293a→301a (21.4%) 285b→294b (6.1%) 286b→294b (21.4%)
65	48301.6	207.0	0.1092	288a→300a (9.7%) 281b→293b (9.2%) 292b→295b (22.8%)
66	48323.4	206.9	0.0556	288a→300a (7.0%) 296a→300a (19.5%) 299a→302a (11.8%) 281b→293b (6.7%) 292b→295b (7.7%)
73	48656.3	205.5	0.1422	291a→301a (7.0%) 292a→301a (14.3%) 284b→294b (7.0%) 285b→294b (14.4%)

Table S13 Selected CAMB3LYP/DKH2 excited states, oscillator strength and monoelectronic transitions for [$Tb_2(dpm)_6(dppeO_2)$] fragment.

State	Energy /cm⁻¹	λ /nm	fosc	Transitions
22	21498.5	465.1	0.0193	299a→ 301a (9.4%) 299a→ 302a (16.4%) 299a→ 303a (33.7%) 299a→ 304a (14.0%) 299a→ 306a (7.4%) 299a→ 309a (9.9%)
24	23021.1	434.4	0.0106	299a→ 301a (6.4%) 282b→ 294b (6.2%) 283b→ 294b (34.6%) 286b→ 294b (36.3%)
25	23605.5	423.6	0.0107	299a→ 301a (80.4%) 299a→ 303a (6.5%)
36	26858.9	372.3	0.0141	299a→ 309a (8.0%) 299a→ 310a (31.1%) 288b→ 294b (13.8%)
79	38647.6	258.7	0.0345	284a→ 300a (8.7%) 296a→ 306a (6.9%) 298a→ 304a (11.2%) 293b→ 298b (13.4%)
83	39363.0	254.0	0.0421	284a→ 300a (26.5%) 285a→ 300a (6.5%) 266b→ 294b (9.1%)
98	42171.1	237.1	0.0238	299a→ 311a (36.7%) 299a→ 314a (13.1%) 299a→ 315a (14.0%)
103	42417.8	235.8	0.0508	299a→ 311a (11.0%) 299a→ 314a (9.6%) 299a→ 315a (16.0%) 299a→ 316a (10.0%)
113	43931.9	227.6	0.0285	299a→ 313a (19.2%) 272b→ 294b (22.7%)
124	45052.1	222.0	0.0200	299a→ 317a (8.8%) 268b→ 294b (7.4%) 269b→ 294b (6.3%) 270b→ 294b (8.6%)